Applied Thermal Engineering 265 (2025) 125587

Contents lists available at ScienceDirect

Applied Thermal Engineering

journal homepage: www.elsevier.com/locate/apthermeng

Research Paper

Optimization of heat transfer using V-shaped staggered ribs for BNCT Solid-State Li targets

Nailiang Zhuang [a,b,*], Kaiwen Qin [a], Langsong Meng [a], Hangbin Zhao [b,c], Xiaobin Tang [a,b]

[a] Department of Nuclear Science and Technology, Nanjing University of Aeronautics and Astronautics, Nanjing 211106, China
[b] Key Laboratory of Nuclear Technology Application and Radiation Protection in Astronautics, Ministry of Industry and Information Technology, Nanjing 211106, China
[c] College of Astronautics, Nanjing University of Aeronautics and Astronautics, Nanjing 211106, China

ARTICLE INFO

Keywords:
Solid Li Target
V-Shaped Staggered Ribs
Rib Height
Rib Angle
Heat Transfer Enhancement

ABSTRACT

As a crucial component of the accelerator device, the lithium (Li) target must withstand high-energy proton beam irradiation while effectively dissipating heat. Consequently, cooling the solid Li target for Boron Neutron Capture Therapy (BNCT) has become an urgent issue to address. In this study, V-shaped staggered ribs are incorporated into the top wall of the cooling channel designed for the BNCT neutron target substrate. The effects of rib height, rib angle, and flow direction on the flow field characteristics and heat transfer characteristics of the cooling channel were numerically investigated. The results indicate that the rib height, rib angle, and flow direction strongly affect the pressure drop, average Nusselt number, velocity distribution, and temperature distribution. Compared to smooth channels, the V-shaped rib channel with a rib angle of 60° and a rib height of 2 mm reduced the maximum surface temperature by 48 %, decreasing it from 200 °C to 104 °C, and achieved a 26 % reduction compared to straight rib channels. Furthermore, the maximum surface temperature can be further minimized by employing backward flow at a specific rib height. While backward flow lowers the temperature, it slightly compromises thermal–hydraulic performance. By effectively reducing surface temperature and enhancing thermal management under high-energy proton beam irradiation, this design minimizes thermal stresses and improves the operational stability and lifespan of BNCT solid-state Li targets, providing a reliable solution for clinical applications.

1. Introduction

Lithium targets have been widely utilized in accelerator-driven boron neutron capture therapy (BNCT) due to their advantages, including high neutron yield, low neutron energy, and ease of moderation [1]. However, the melting point of the solid lithium target is relatively low (only 453 K), and the heat deposited by the high-energy proton beam bombarding the lithium target cannot be dissipated in time, which may cause melting and damage to the neutron target station, affecting its lifetime. In addition, the beam intensity and energy required for BNCT continues to increase with the growing clinical demand [2], resulting in a corresponding increase in the thermal load on solid lithium targets. Therefore, the heat dissipation capability of the neutron target station substrate is one of the critical factors [1,3], and solving the heat dissipation problem of solid Li targets has become a research focus and challenge.

Currently, the Li targets used in accelerator-driven BNCT mainly fall into three main categories: static solid targets, rotating solid targets, and liquid targets. For static solid targets, heat dissipation is typically achieved by incorporating cooling channels in the neutron target station substrate and by increasing the interaction area between the proton beam and the neutron target station. Rotating solid targets aim to reduce the heat flux of the neutron target station by increasing the interaction area between the proton beam and the neutron target station through rotation. To increase the heat removal capability of a solid Li target substrate, researchers have proposed various cooling structure designs. Carl Willis [4] and Nakamura [5] both suggested using a conical solid Li target to increase the irradiation area of the proton beam, thereby improving the heat removal capability of the neutron target station. Their studies have identified that the thermal loading of the neutron target station structure is a significant factor contributing to reduced efficiency during treatment, as illustrated in Fig. 1(a) and Fig. 1(b). Wang et al.[6] introduced a neutron target station with an edge-cooling structure for a transportable accelerator-driven neutron source, as illustrated in Fig. 1(d). The edge-cooling target effectively maintains a

* Corresponding authors.
E-mail address: zhuangnailiang@nuaa.edu.cn (N. Zhuang).

https://doi.org/10.1016/j.applthermaleng.2025.125587
Received 13 July 2024; Received in revised form 17 December 2024; Accepted 15 January 2025
Available online 16 January 2025

Nomenclature

A_f	Wetted surface area(m^2)	Nu	Nusselt number
D_h	Equivalent diameter	T_{max}	Maximum temperature(K)
f	Friction factor	T_w	Wall temperature (K)
Re	Reynolds numbers	T_f	Inlet temperature (K)
L	Channel length(mm)	PEC	Comprehensive evaluation factor
θ	Angles(°)	v_{avg}	Average velocity (m/s)
ΔP	Pressure drop(Pa)	V_f	Volume of the liquid (m/s)
h	Heat transfer coefficient($W/(m^2 \cdot K)$)	μ	Dynamic viscosity(Pa/s)
P_{out}	Outlet pressure(Pa)	λ	Thermal conductivity
P_{in}	Inlet pressure(Pa)	ρ	Density(kg/m^3)
q	Heat flux (W/m^2)	T_{in}	Inlet temperature (K)
		T_{out}	Outlet temperature (K)
		η	Thermal-hydraulic performance factor

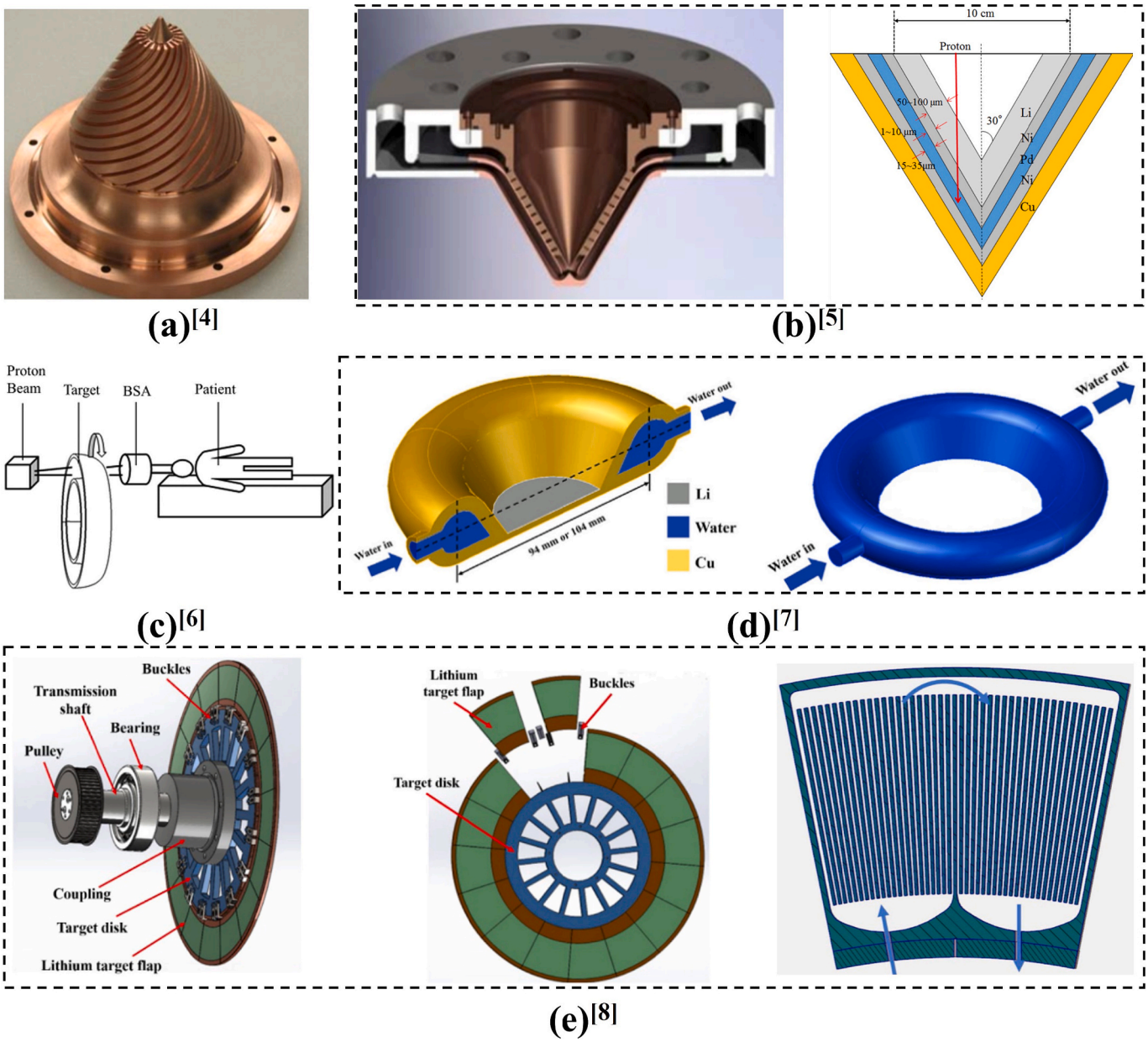

Fig. 1. Neutron target station structures for enhanced heat dissipation in literatures.

stable temperature while ensuring the required intensity of forward-emitting neutrons with minimal attenuation. This innovation provides a novel approach to the cooling design of neutron target stations. Wang et al.[7] designed a curved Li target in a half-tire shape that rotates around its center, as depicted in Fig. 1(c). Calculations indicate that this design produces a more concentrated neutron beam with improved forward directionality, outperforming the flat target. For a 50 kW proton beam, the maximum temperature of the curved Li target reaches only 100 °C, which meets its heat dissipation requirements. Hu et al.[8] developed a rotating target structure, with the target's rotating motion, the rotating target disk, and the channel structure in the flap depicted in Fig. 1(e). Heat transfer simulations using the Computational Fluid Dynamics (CFD) method were conducted with Gaussian and uniform beams in the rotating target system. The maximum temperatures of the Li remained below its melting point, demonstrating the effectiveness of the rotating target structure in cooling. However, problems with the channel structure and rotation led to the formation of local hot spots. In addition, the high rotational speed of the target requires superior mechanical properties.

Although significant progress has been made in the design and optimization of cooling structures for neutron target stations, existing solutions still face critical limitations. These include insufficient mitigation of localized thermal hotspots, mechanical challenges associated with high-speed rotation, and a lack of approaches that comprehensively address both thermal and structural performance. Therefore, it is necessary to propose an efficient cooling structure with superior heat dissipation performance to ensure both improved thermal management and operational reliability for accelerator-driven BNCT systems.

Currently, researchers have proposed various methods to enhance heat transfer performance, including channel geometry optimization [9], surface enhancement techniques [10], nanofluid technology [11], and phase-change heat transfer technology [12], as shown in Fig. 2. Among these, channel geometry optimization is one of the most widely studied approaches for heat transfer enhancement. Its core principle is to modify the flow path and boundary conditions to increase turbulence intensity, reduce the thermal boundary layer, and ultimately improve heat transfer efficiency. Common geometry optimization strategies include microchannel designs [13], straight ribs [14], wavy structures [15], and porous channels [16]. While these methods demonstrate significant improvements in heat transfer, they also face several limitations [17]. For example, although microchannel structures are known for their high heat transfer performance, they are complex to manufacture and prone to clogging or flow instability due to particle deposition [18]. Similarly, designs such as wavy or ribbed structures are effective in disturbing the flow field but often result in significant pressure drop penalties, reducing the overall energy efficiency of the system [19]. Achieving an optimal balance between heat transfer enhancement and pressure drop remains a critical challenge in this field. Surface enhancement techniques aim to improve the interfacial heat transfer efficiency by introducing microstructures or coatings on heat exchange surfaces. Although these techniques achieve remarkable results in improving heat transfer performance, their durability in high-temperature, high-pressure, or corrosive environments is often limited [20], and the complexity of surface processing increases their cost. Nanofluid technology has become a research hotspot due to its superior thermal conductivity and tunable fluid properties, but its practical engineering applications are limited by challenges such as particle dispersion stability, long-term reliability, and economic feasibility [21]. Phase-change heat transfer technology shows great potential in the synergistic design of thermal storage and heat transfer; however, its performance is often limited by phase change rates and heat flux density compatibility, making it difficult to achieve stable and efficient heat transfer under dynamic and complex operating conditions [22]. Despite the advantages of the above methods, there are still certain bottlenecks in practical applications. On the one hand, existing methods struggle to achieve a desirable balance between high heat transfer performance and

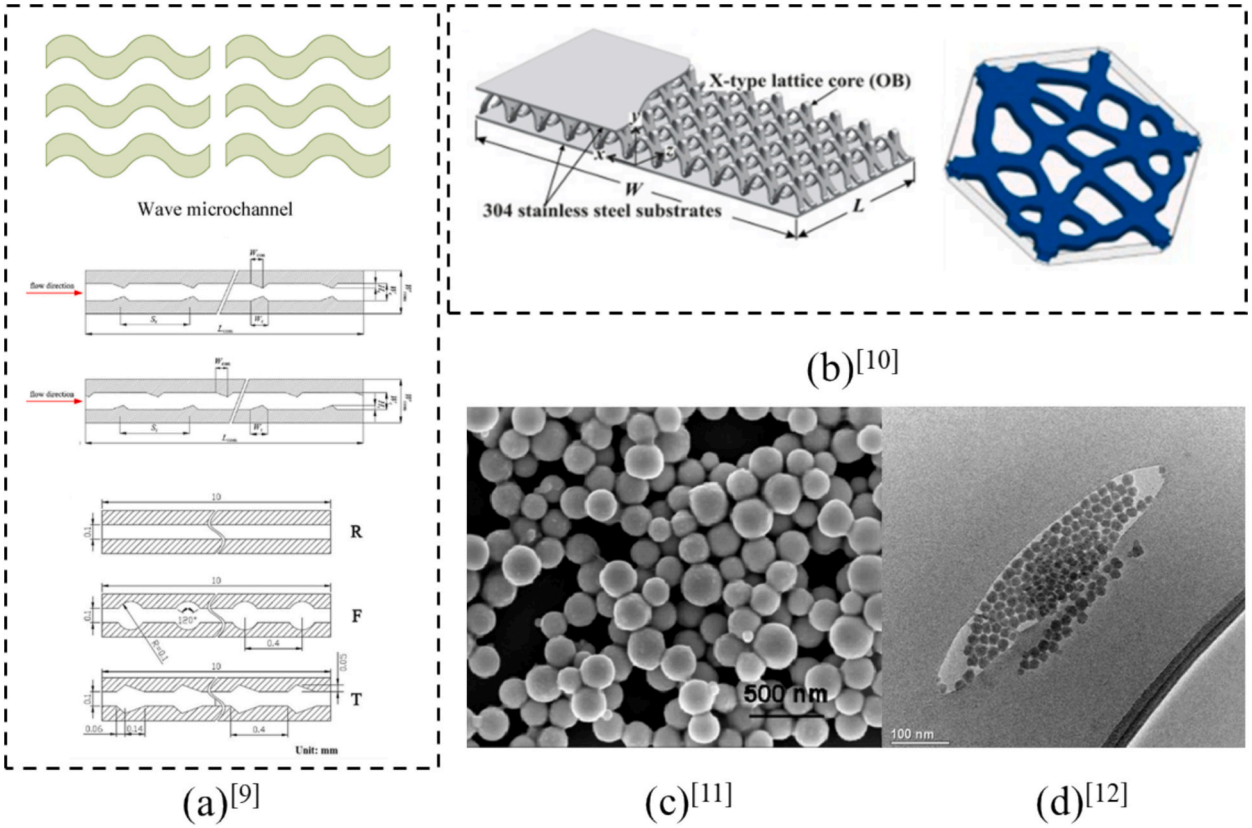

Fig. 2. Some heat transfer enhancement methods in literatures.

low pressure drop increments. On the other hand, these methods often fail to meet the requirements of complex flow fields and to adapt to different operating conditions.

The ribbed structure, as a practical method to enhance heat transfer, has been widely applied in the fields of aerospace [23], energy engineering [24], and nuclear technology [25]. Promvonge et al. [26] studied the turbulent flow and heat transfer in a square duct with 60° V-shaped ribs on two opposite heated walls (Fig. 3(a)). They examined the effect of blockage ratios (e/D) on heat transfer at Reynolds numbers of 10,000–25,000. The ribs created counter-rotating vortices (P-vortices), that enhanced heat transfer by impingement and reattachment flows. Increasing the blockage ratio increased both heat transfer and friction losses. At lower Reynolds numbers, a BR of 0.0725 achieved a thermal performance of ~ 1.8, with a heat transfer rate four times that of a smooth channel. Sriharsha et al. [27] compared heat transfer performance between straight ribs and 60° V-shaped broken ribs (Fig. 3(b)), and found superior performance and lower pressure drop with the latter, although increased rib height reduced effectiveness. Liu et al.[28] designed a saw-like microchannel (Fig. 3(c)) that disrupted the thermal boundary layer, significantly improving convective heat transfer. Zhang et al.[29] analyzed flow and heat exchange in a channel with V-shaped disturbance ribs (Fig. 3(d)) at different guide angles. The highest heat exchange efficiency occurred at 47.25°, while optimal cooling efficiency was at 31.57°. Wu et al.[30] investigated turbine blade passages with V-shaped discrete ribs (Fig. 3(e)), and found improved heat transfer performance and temperature uniformity. Optimized ribs increased the Nusselt number by 35.75 % and the comprehensive heat transfer coefficient by 28.95 % compared to transverse ribs at a Reynolds number of 30,000. It can be seen that in more specific engineering applications, the addition of ribs to channels can disrupt the development of the thermal boundary layer, improving convective heat and mass transfer, and significantly improve the heat transfer efficiency of the equipment.

Recently, V-shaped staggered ribs were also proposed to enhance the heat dissipation performance of neutron target stations. Yoshihashi S. et al.[31] proposed to improve the heat dissipation performance of neutron target stations by incorporating V-shaped staggered ribs into the smooth straight channel structure, as shown in Fig. 4. They analyzed the heat dissipation performance of both smooth straight channel and V-shaped staggered rib channels. The results indicated that the heat dissipation performance of the fluid channel with V-shaped staggered ribs is twice that of the smooth structure, and the heat transfer coefficient is 2.4 times higher. However, this study did not consider the effects of fluid flow regimes or the influence of the structural parameters of the V-shaped ribs, such as rib height, spacing, and angle, which were not systematically analyzed.

In the design of accelerator-driven BNCT neutron targets, microchannels and various types of fins and ribs can be used to increase the heat removal capacity. However, detailed designs and calculations are required for the cooling structures of BNCT solid Li targets with different proton beam currents and energies. In addition, the types and structural parameters of the fins and ribs need to be investigated and analyzed based on different proton beam currents. Therefore, in the context of BNCT solid lithium targets, it is essential to investigate the combined effects of flow velocity, rib geometry, and arrangement on heat transfer performance and pressure drop.

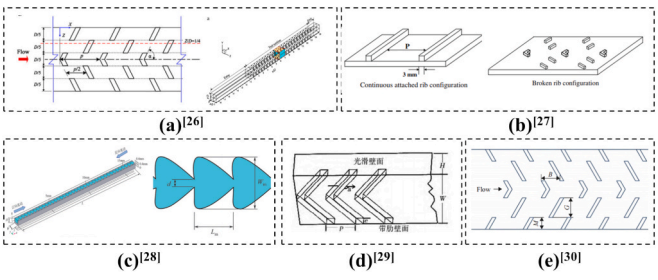

(a)[26] (b)[27] (c)[28] (d)[29] (e)[30]

Fig. 3. Rib structures for enhanced heat dissipation in literatures.

To solve this problem, the present study proposes a V-shaped staggered rib structure designed in the substrate of the neutron target station substrate by optimizing the rib geometry and arrangement. A simulation study of the flow field and heat transfer characteristics of the V-shaped staggered ribs flow channel structure was carried out. The effects of the V-shaped staggered rib heights, the angle between the rib and the side wall, and the flow direction on flow and heat transfer characteristics under different operating conditions were investigated. The paper is structured as follows, first, the design of the neutron target station with V-shaped staggered ribs, and simulation method were briefly introduced. Then, the quantitative influence of the geometric parameters and flow direction of the V-shaped staggered ribs on the flow field, pressure drop, and heat transfer characteristics were systematically discussed. The flow and heat transfer characteristics in smooth channel and the straight-rib channel were also studied as a comparison and reference. The influencing laws and the influencing mechanism of the V-shaped ribs are discussed and analyzed in detail.

2. The neutron target station and numerical method

2.1. The neutron target station with V-shaped staggered ribs

To enhance the heat transfer performance of the BNCT Li target substrate structure, a V-shaped staggered rib structure on the top wall of the microchannel structure was designed in this study, as depicted in Fig. 5. The neutron target station substrate is constructed from a copper plate measuring 124 mm in length, 120 mm in width, and 9 mm in thickness, featuring 10 channels that are 10 mm wide and 5 mm high, with V-shaped staggered ribs arranged on the top walls of these channels.

To simplify the numerical calculations, the multi-channel copper plate structure was reduced to a single-channel model, as shown in Fig. 5 (c)and (d). The V-shaped staggered rib structures have a channel length of 40 mm, with 40 mm smooth channels at both the inlet and outlet to minimize entry and exit effects, resulting in a total length of 120 mm. The heating area, located on the copper plate above the V-shaped staggered rib structures, is 40 mm long and 10 mm wide, using a uniform heat flux density. Fluid enters the channel from two directions, as indicated by the blue arrows in Fig. 5(d). The effects of the forward and backward flow directions on channel flow and heat transfer will be analyzed. The channel has a width of 10 mm, a height of 5 mm, and wall thicknesses of 2 mm at the top and bottom and 1 mm at the sides. The rib thickness is 1 mm, and rib height is denoted as h, the rib angle as θ, as indicated in Fig. 5(d). The distance between ribs on the same side is 3.8 mm, and between ribs on opposite sides is 1.4 mm. In addition, channels with smooth structures and straight rib structures were analyzed as a comparison and reference to evaluate the heat dissipation performance of the V-shaped staggered rib channels.

2.2. Numerical simulation method

2.2.1. Boundary condition

Assuming the proton beam is uniformly distributed and the target station operates in an adiabatic environment, the deposited energy in the simulation is set to 25 kW. The proton beam parameters, proton energy of 2.5 MeV, beam current of 10 mA, and beam spot radius of 5 cm, are based on the specifications of the proton accelerator used by Neuboron Medtech Ltd [32]. These parameters correspond to a heat flux density of 3.183 MW/m2. The inlet fluid velocity is set to 2 m/s, corresponding to a total flow rate of 12 L/min, with the inlet fluid temperature maintained at 293.15 K. The outlet condition is defined as a pressure outlet. A constant heat flux density of 3.183 MW/m^2 is applied to the top surface of the channel to simulate the heat deposition resulting from proton bombardment on the lithium target.

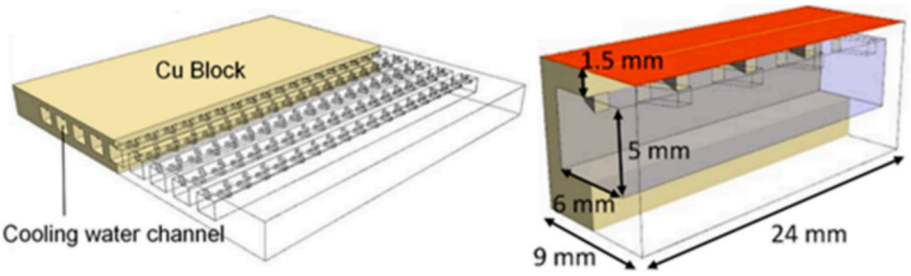

Fig. 4. The neutron target station with V-shaped staggered ribs [31].

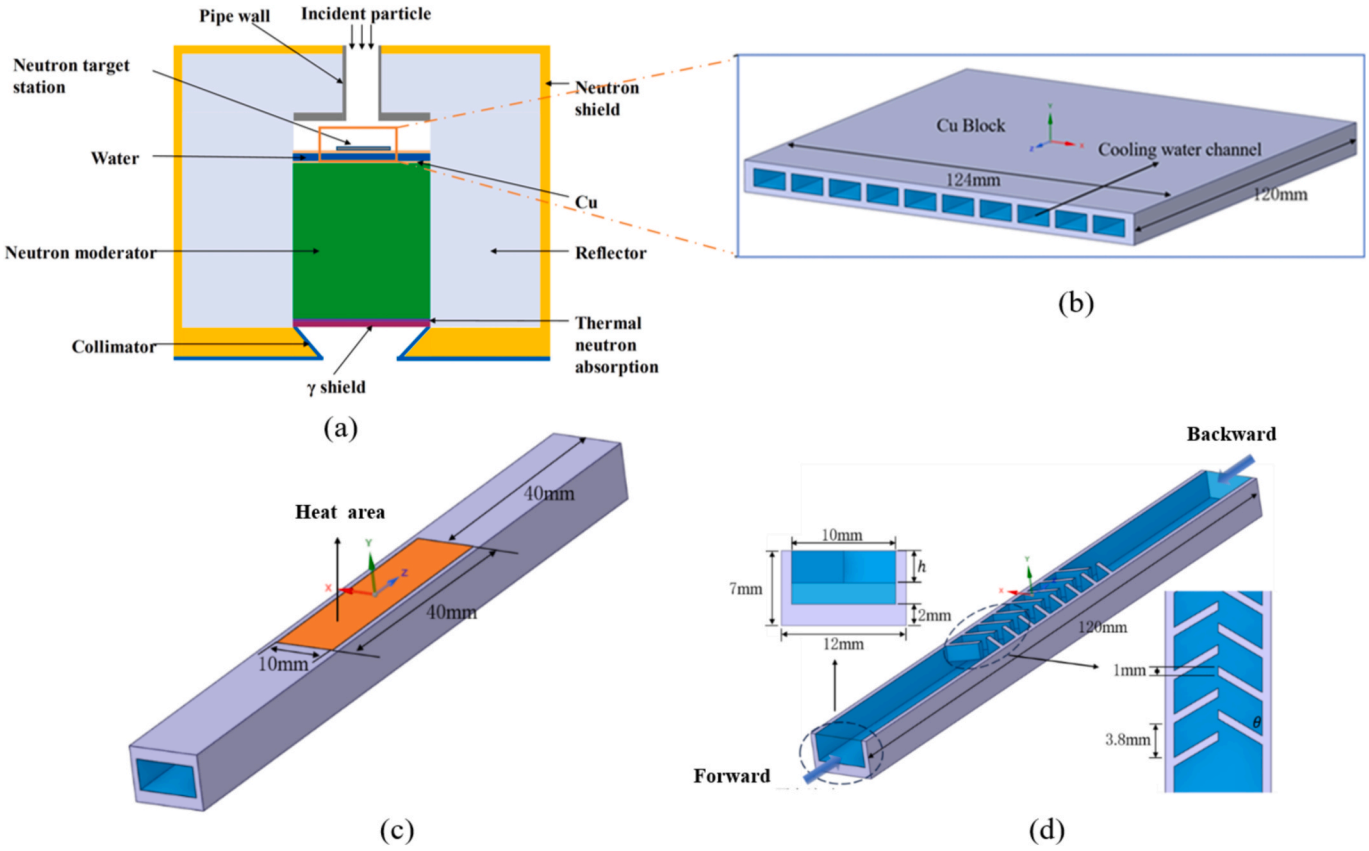

Fig. 5. Schematic diagram of target and V-shaped staggered rib channel structure.

Based on the recommendation of Ref.[33], SST k-ω model is more accurate, and reliable, incorporating modification for low Reynolds number effects, compressibility, and shear flow propagation, which is very suitable for simulating complex internal flow field of V-shaped staggered rib channel. The momentum equation is discretized using the second-order upwind scheme, while the energy equation is discretized using the second-order upwind scheme. Default values are assigned to other parameters. Convergence criteria are established based on normalized residuals of the momentum, energy, and other equations being less than 10^{-5}, ensuring the maximum surface temperature remains stable.

2.2.2. *Grid independent verification*

The grid independence analysis was performed on a single-channel model with V-shaped staggered ribs. The channel structure had V-shaped staggered rib parameters of h = 3 mm and θ = 60°. Local grid refinement was applied to the V-shaped staggered rib channel structure section by introducing localized grid sizes to increase grid densification in that specific area. In the fluid boundary layer region, five layers of boundary layers were included to capture detailed fluid information, as illustrated in Fig. 6. Five kinds of grid structures were established in this study, with grid numbers of 330,000, 620,000, 1,120,000, 2,230,000,

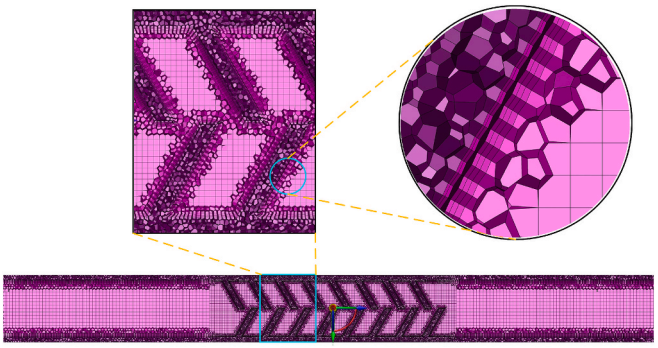

Fig. 6. The grid information of the V-shaped staggered rib channel.

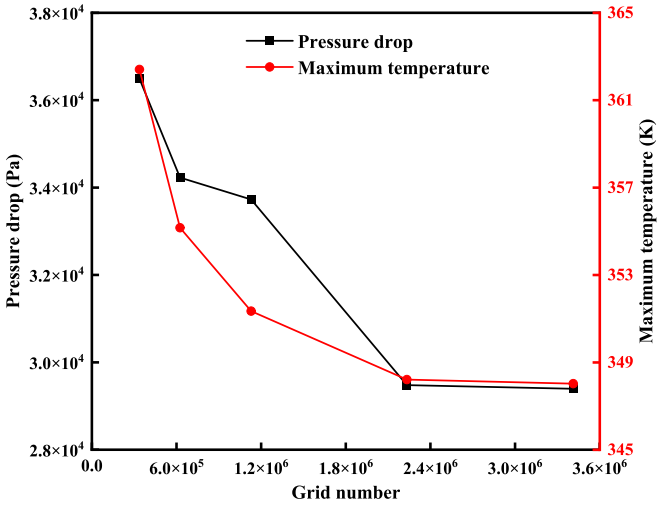

Fig. 7. The maximum surface temperature and pressure drop with grids number.

and 3,410,000, respectively. An inlet fluid velocity of 2 m/s was chosen for verification. Using the maximum surface temperature (T_{max}) and the pressure drop (ΔP) between the inlet and outlet for the grid number with 3,410,000 grids as the benchmarks, the results are shown in Fig. 7.

It can be seen that with a grid number of 1,120,000, the change in the maximum surface temperature and the pressure drop between the inlet and outlet (ΔP) are 1.3 % and 15.6 % respectively. In contrast, with a grid number of 2,230,000, the changes in the maximum surface temperature and the pressure drop between the inlet and outlet are 0.4 % and 0.6 %, respectively. Considering that these parameters change the least when the number of grids is 2,230,000, and considering the simulation results' accuracy and efficiency, the grid number of 2,230,000 was selected for numerical simulation calculations in this study.

2.3. Flow and heat transfer performance evaluation parameter

To analyze the effect of rib heights, angles, and fluid flow direction on the flow and heat transfer performance of the solid Li target substrate, various parameters are introduced to characterize flow and heat transfer properties.

2.3.1. Pressure drop characteristic

The expression of Reynolds number (Re) is:

$$\mathrm{Re} = \frac{\rho v_{ave} D_h}{\mu} \tag{1}$$

where ρ represents the fluid density, D_h denotes the hydraulic diameter, v_{ave} is the average fluid velocity, and μ stands for the dynamic viscosity.

The calculation method for the hydraulic diameter (D_h) is as follows:

$$\mathrm{D}_h = \frac{4V_f}{A_f} \tag{2}$$

where V_f represents the volume of the liquid, and A_f denotes the wetted surface area.

When evaluating the overall performance of the channel, it is essential to consider both the heat transfer characteristics and the pressure drop of the fluid within the channel. The calculation method for pressure drop is as follows.

$$\Delta P = P_{in} - P_{out} \tag{3}$$

where P_{in} is the inlet pressure and P_{out} is the outlet pressure.

The friction factor f is a dimensionless parameter introduced in fluid flow calculations. Its value is related to the Reynolds number and relative roughness, and it can be calculated using the following formula:

$$f = \frac{2\Delta P D_h}{\rho v_{ave}^2 L} \tag{4}$$

where L denotes the channel length.

2.3.2. The convective heat transfer coefficient and Nusselt number

The convective heat transfer coefficient is a parameter that describes the ability of heat transfer between a fluid and a solid interface. The average convective heat transfer coefficient is used in this study, and the calculation formula is as follows:

$$h = \frac{q}{T_w - T_f} \tag{5}$$

where q is the average heat flux density of the pipe wall, T_w is the temperature of the inner wall, T_f is the average temperature of the fluid in the channel, the formula is as follows $T_f = \frac{T_{in}+T_{out}}{2}$, T_{in} is the inlet temperature, T_{out} is the outlet temperature.

The Nusselt number (Nu) reflects the heat transfer performance of the fluid boundary layer in the process of fluid heat transfer. The average Nusselt number is used in this study, and the calculation formula is as follows:

$$Nu = \frac{hD_h}{\lambda} \tag{6}$$

where λ is the thermal conductivity at the average temperature of the fluid.

2.3.3. Thermal-hydraulic performance factor

The thermal–hydraulic performance factor η is used to comprehensively evaluate the performance of the rib channel [5], which takes into account both heat transfer and pressure drop loss, and the calculation formula is as follows:

$$\eta = \frac{Nu/Nu_0}{(f/f_0)^{1/3}} \tag{7}$$

where Nu_0 and f_0 are the Nusselt number and the friction factor of a smooth channel (with zero rib height), respectively. It is generally considered that when the value of η exceeds 1, the heat transfer enhancement by the ribs is effective. The higher the value of η, the better the heat transfer enhancement effect of the ribs.

3. Results and discussion

In this section, the effect of rib heights (h) and angles (θ) of V-shaped staggered ribs, and the flow direction on the flow and heat transfer performance of the cooling channels of the neutron target station will be systematically discussed. The flow field distribution, pressure drop, maximum surface temperature, temperature distribution, Nusselt number, and thermal–hydraulic performance factors will be analyzed.

3.1. Effect of rib height

In this section, the effect of rib heights on the flow and heat transfer characteristics in channels with V-shaped staggered ribs when the rib angle is fixed at 60° was studied. Straight rib channels and smooth channels and were also analyzed and used as references. A total of 19 different model structures were designed, with specific parameters detailed in Table 1.

3.1.1. Flow field characteristic

The pressure drops of the V-shaped staggered rib channels and straight rib channels with different rib heights are illustrated in Fig. 8. It

Table 1
Structural parameters of channels with different rib heights.

Type	Number	Rib heights	Rib angles	Flow direction
Smooth channel	1	—	—	—
Straight rib channel	2–10	0.5–4.5	—	—
V-shaped staggered rib channel	11–19	0.5–4.5	60°	forward

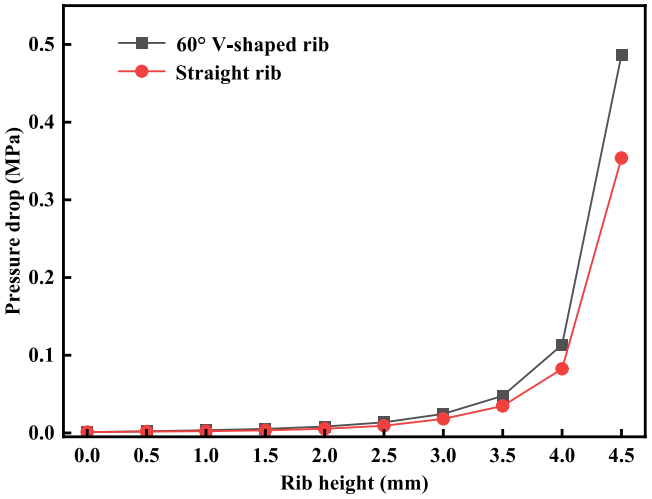

Fig. 8. The effect of rib heights on pressure drops.

can be seen that the pressure drop of V-shaped staggered rib channels and straight rib channels increases slowly at first and then rapidly as the rib height increases. This phenomenon occurs because as rib height increases, the flow area for the fluid decreases, leading to an intensification of flow field vortices (refer to flow field characterization in Fig. 9), increasing pressure drop. The increase in pressure drop for the straight rib channel is less than that for the V-shaped rib channel. For example, the pressure drop in a V-shaped staggered rib channel is approximately 7.5 times that of a smooth channel and 1.5 times that of a straight rib channel, when the rib height is 2 mm.

The velocity distribution of V-shaped staggered rib channels and straight rib channels is shown in Fig. 9(a), with the x-z plane (y = 6.5 mm) positioned 0.5 mm from the top wall of the channel. It can be seen that the fluid velocity is higher in the central region of both channels and lower near the side walls. In the V-shaped staggered rib channel, the staggered arrangement of the rib creates a high velocity flow region near the tip of the rib. The velocity in the x-axis direction exhibits a periodic change, alternating between fast and slow. When leaving the V-shaped staggered rib region, the flow velocity in the central region is lower than that near the sidewall region. In the straight rib channel, the fluid velocity decreases significantly after passing through the first rib and gradually recovers and becomes uniform. In the outlet section, the fluid flow velocity in the central region of the V-shaped rib channel remains lower than the flow velocity near the sidewall region.

The velocity distribution in the x-z plane for the V-shaped staggered rib channels with different rib heights is shown in Fig. 9(b). As the rib height increases, the flow velocity in the central region of the channel gradually increases, forming a wave-like region that enhances the fluid mixing effect. The fluid with high velocity concentrates in the middle region of the channel. In addition, the velocity on the windward side of the ribs is larger, and the flow velocity on the back is smaller. As the rib height increases, the difference between the fluid velocity in the central of the channel and the fluid velocity at the edge of the channel increases.

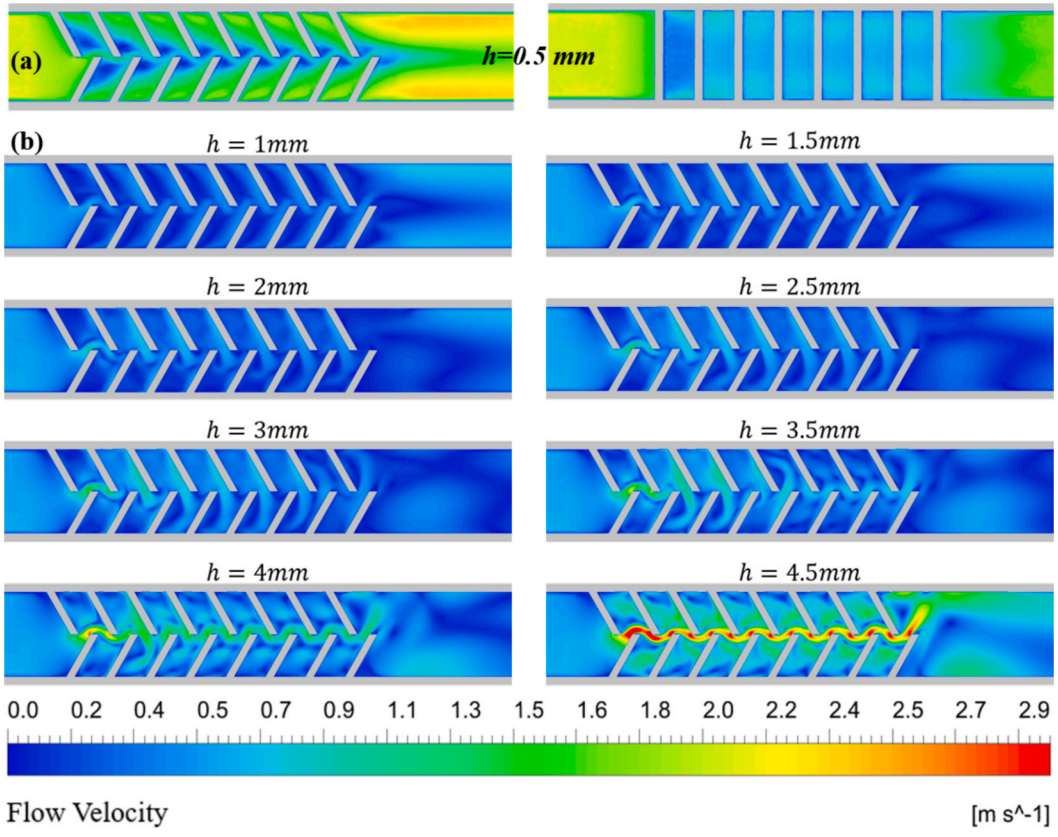

Fig. 9. The effect of rib heights on velocity magnitude distribution (a) V-shaped staggered rib channel and straight rib channel (h = 0.5 mm, y = 6.5 mm) (b) V-shaped staggered rib channels with different rib heights (y = 7.5 mm).

The stronger the flow layer shear and fluid mixing, the more intense the vortex detachment at the edge of the rib. Similar phenomenon is also reported in Ref. [34,35]. Near the inlet, the flow velocity on the left side of the rib tip is significantly higher than that on the right side. The fluid flow velocity near the left wall of the rib is higher than the right wall due to the formation of counter-clockwise vortices in the top part of the central region and clockwise vortices in the lower part of the central region as the fluid passes through the rib. The velocity distribution shows that the fluid velocity distribution is more uniform in the inlet section, whereas the flow velocity distribution becomes non-uniform after flowing out of the V-shaped rib structure. As the rib height increases, the average flow velocity of the fluid in the channel gradually increases.

The velocity distribution of straight rib channels with different rib heights is shown in Fig. 10. It can be seen that as the rib height increases, the flow velocity at 0.5 mm from the top wall surface first decreases and then gradually increases. The flow velocity near the right side of the rib is lower than that on the left side, and along the z-axis, the flow velocity shows a gradually increasing trend. As the rib height increases, the low flow velocity region in the inlet section near the first rib gradually expands. In contrast, the flow velocity distribution of the straight rib structure is more uniform, while the V-shaped staggered rib structure creates a high-velocity flow region resembling a wave shape.

3.1.2. Heat transfer characteristic

The maximum surface temperature of the neutron target station's substrate for V-shaped staggered rib channels and straight rib channels at different rib heights is illustrated in Fig. 11 (with an inlet fluid velocity of 2 m/s). A rib height of 0 mm represents a smooth channel without ribs. It can be seen that the maximum surface temperature of the V-shaped staggered rib channel consistently remains lower than that of the straight rib channel. The maximum surface temperatures are below the melting point of the metal Li. In the V-shaped staggered rib channel, the rate of temperature decrease initially slows down and then gradually increases. The temperature difference between the staggered and straight rib channels varies from a maximum of 44 °C to a minimum of 26 °C. In terms of maximum surface temperature, the performance of the V-shaped staggered rib channel is significantly superior to that of the straight rib channel. At a rib height of 2 mm, the maximum surface temperature of the V-shaped staggered rib channel is decreased by 48 % compared to the smooth channel and by 26 % compared to the straight rib channel. For the V-shaped staggered ribs, the maximum surface temperature can be decreased to 72 °C at a rib height of 4.5 mm. However, consider the pressure drop at the inlet and outlet reaches 0.11 MPa when rib height is increased to 4 mm. Therefore, simply increasing rib height to reduce the temperature is not advisable in practical applications.

As shown in Fig. 12, there is a significant difference in the effect of rib height on the average Nusselt number (Nu) for V-shaped staggered rib channels and straight rib channels. For straight rib channels, the

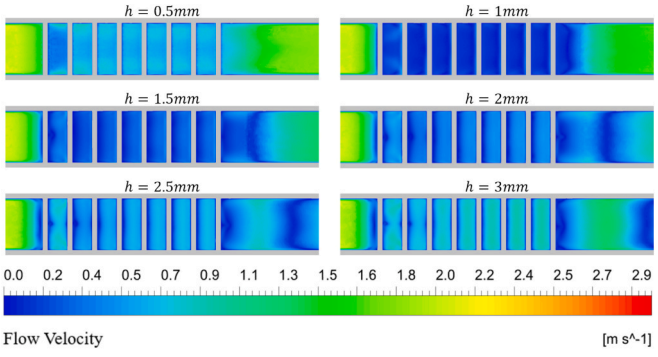

Fig. 10. Effect of rib height on velocity distribution of straight rib channel.

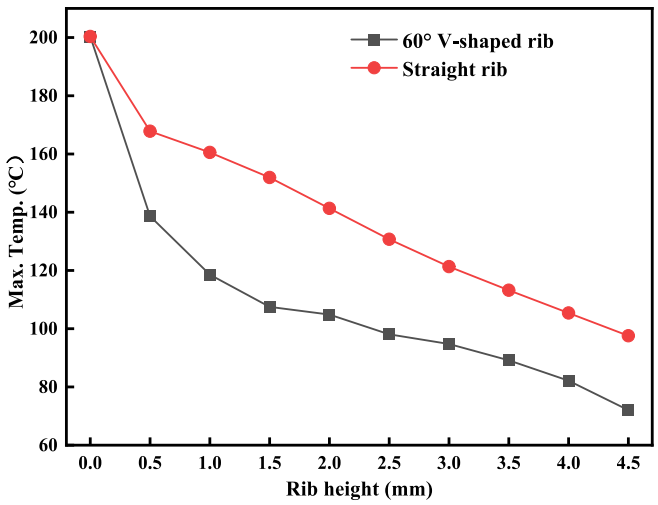

Fig. 11. The effect of rib heights on the maximum surface temperature.

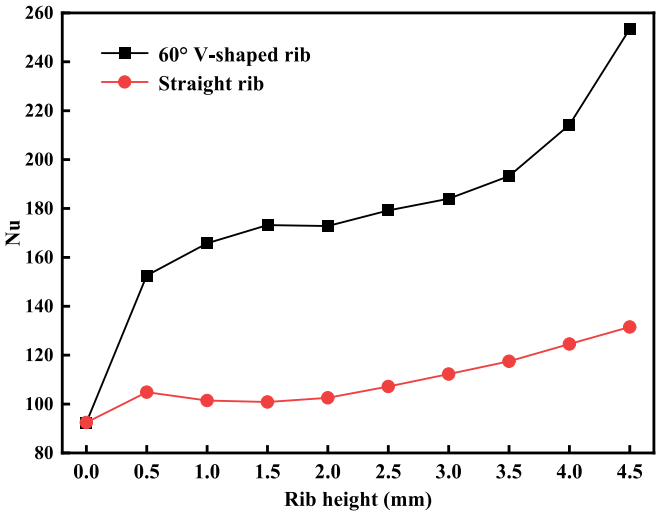

Fig. 12. The effect of rib heights on the average Nu.

average Nu initially decreases and then increases, reaching a minimum at a rib height of 1.5 mm, but it remains higher than the average Nu of a smooth channel. For V-shaped staggered rib channels, the average Nu generally increases with rib height, with a decreasing growth rate from 0.5 mm to 1.5 mm, and the average Nu at 2 mm is lower than at 1.5 mm and 2.5 mm. Overall, the average Nu for V-shaped staggered rib channels is consistently higher than that of straight rib channels. For example, at a rib height of 2 mm, the average Nu of V-shaped staggered rib channels increase by 87 % compared to the smooth channel and by 69 % compared to straight rib channels.

As shown in Fig. 13(a), the temperature distribution on the top wall surface of the V-shaped staggered rib channel indicates that the temperature gradually decreases as the rib height increases. The high temperature region shifts towards the outlet, with higher temperatures near the outlet. In addition, the temperature in the central region is higher than that near the sidewall surface. The temperature distribution is closely coupled to velocity field (as shown in Fig. 9). It can be seen that the temperature on the windward side of the ribs is lower, and the temperature on the back is higher. According to the analysis of flow field distribution above (Fig. 9), as the rib height increase, the flow layer shear and fluid mixing become stronger, the vortex detachment at the edge of the rib become more intense, which enhance the heat and mass transfer capability of cooling channel [35,36].

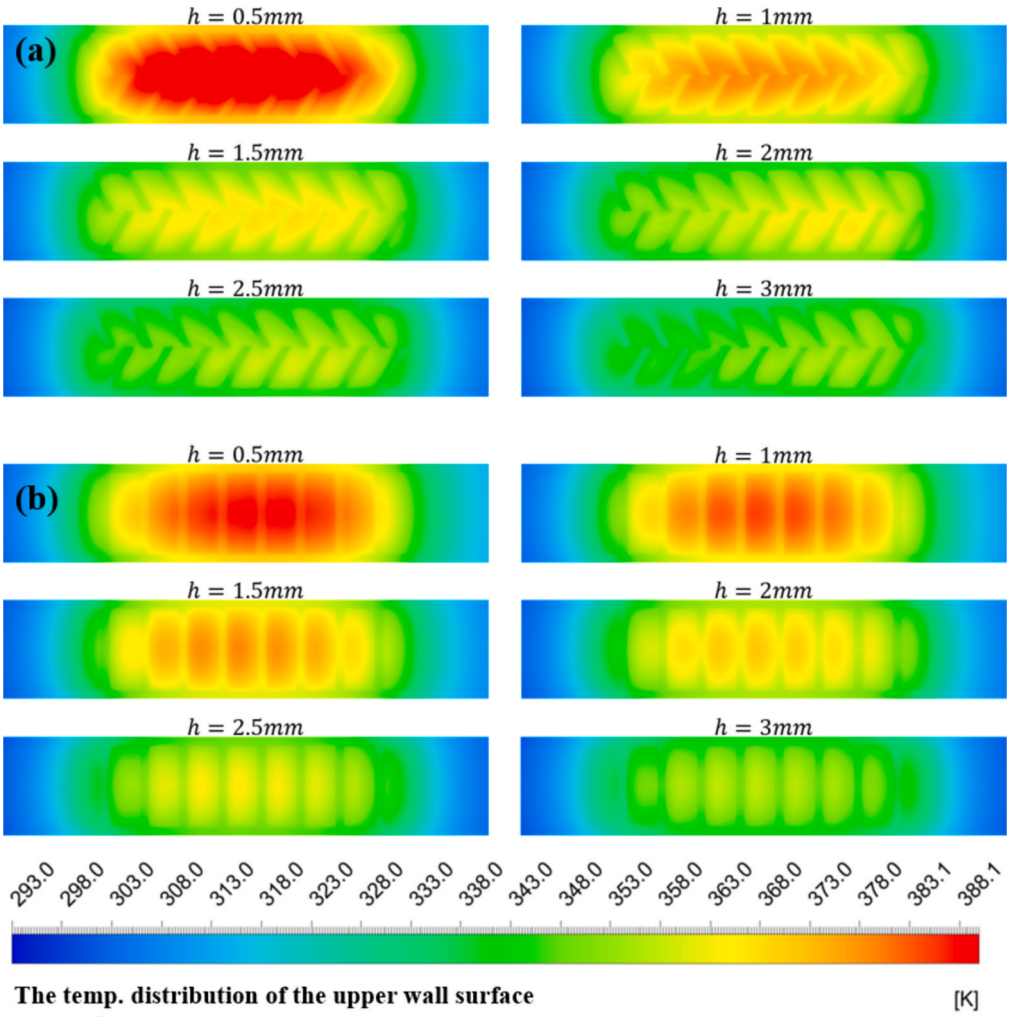

Fig. 13. The effect of rib heights on the surface temperature distribution of (a) V-shaped staggered rib channels and (b) straight rib channels.

Fig. 13(b) displays the temperature distribution on the top wall surface of the straight rib channels. In contrast to V-shaped staggered rib channels, the temperature in the heating region of straight rib channels is more uniform, with the high-temperature region concentrated in the central region in a symmetrical distribution. Despite the lower temperature on the top wall surface of the staggered rib channel, the temperature distribution of the straight rib is more uniform. Comparing the velocity profiles of the straight ribs, although the flow velocity near the rib at the outlet is lower than in the central region, it does not impede the cooling of the top wall surface. The comparison of the velocity distribution of the staggered ribs reveals that the temperature of the top wall surface in the central region remains relatively stable due to the wave-like high velocity flow zone.

3.1.3. *Thermal-hydraulic performance factor*

The effect of rib height on the thermal–hydraulic performance factor (η) of V-shaped staggered ribs and straight ribs is shown in Fig. 14. It can be seen that the thermal–hydraulic performance factor decreases with increasing rib height for both types of rib channels. For V-shaped staggered rib channels, the thermal–hydraulic performance factor drops below 1 when rib height reaches 2.5 mm. In contrast, for straight rib channels, the thermal–hydraulic performance factor is less than 1 when rib height is 1 mm. In addition, the rate of decrease in the thermal–hydraulic performance factor tends to stabilize for straight ribs. For example, at a rib height of 2 mm, the thermal–hydraulic performance factor for V-shaped staggered rib channels is 44 % higher than that for straight rib channels.

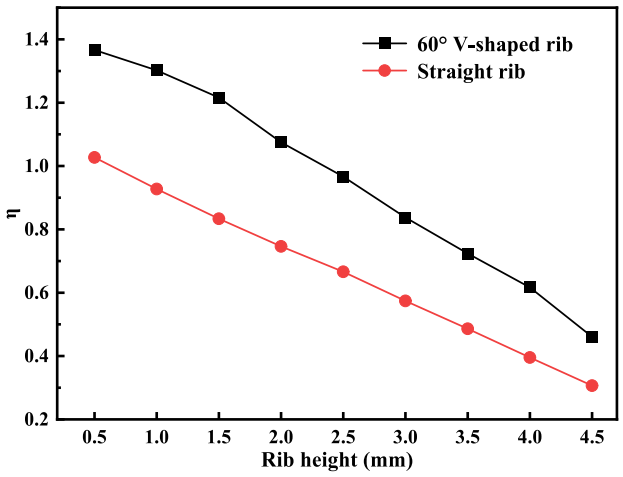

Fig. 14. The effect of rib heights on thermal–hydraulic performance factor.

To sum up, the effect of rib height on pressure drops, average Nu number, surface temperature, flow field and heat transfer capability is significant. The mechanism analysis shows on the one hand, the increase of rib height reduces the flow area and increases the general flow rate. On the other hand, the difference of flow velocity distribution in the

channel is greater, the velocity in the central of the channel is greater, the shear of the flow layer is more intense, and the fluid mass exchange after the vortex falls off the rib edge is more intense, which further improves the mass and heat exchange in the channel, especially in the central area, so as to achieve enhanced heat transfer.

In terms of the maximum surface temperature, increasing rib height is effective in decreasing the temperature, and the temperature continues to decrease as the rib height increases. However, pressure drop also increases significantly as the rib height increases. The average Nusselt number (Nu) increases significantly with the increase in rib height for V-shaped staggered ribs, while the average Nu does not change significantly for straight ribs. According to the analysis of thermal–hydraulic performance factors, when the rib height exceeds 2 mm, V-shaped staggered ribs become ineffective in improving heat transfer in the channel, although the surface maximum temperature decreases significantly. A comprehensive analysis shows that when the rib height is 2 mm, the heat transfer effect of V-shaped staggered ribs is optimal, and the maximum surface temperature can be reduced to 104 °C.

3.2. Effect of rib angle

As mentioned above, when analyzing the effect of rib height, the rib angle is fixed at 60°. In this section, the effect of rib angles (60°, 45°, 37.5°, 30°) on the flow and heat transfer characteristics in channels will be discussed. Moreover, the combined effect of rib angle and rib height the with rib heights ranging from 0.5 mm to 4.5 mm will also analyzed. A total of 36 model structures of V-shaped staggered rib channels were established, and the specific parameters are shown in Table 2.

3.2.1. Flow field characteristic

As shown in Fig. 15, the effect of the V-shaped staggered rib angles on pressure drop at an inlet flow velocity of 2 m/s is significant. Taking a rib height of 2 mm as an example, four conditions with angles of 30°, 37.5°, 45°, and 60° were studied. The results indicate that as the angle of the V-shaped staggered ribs increases, the pressure drop increases continuously, reaching a peak at 45°, and then rapidly decreases. Under different rib heights conditions, the effect trend of the V-shaped staggered rib angles on pressure drop is similar. The higher the height of the rib, the more significant the effect of the rib angle. Specifically, as rib height increases, the effect of rib angles on pressure drop becomes more significant, both in absolute and relative terms. Of the four rib angles studied, 45° results in the highest pressure drop, while 60° results in the lowest pressure drop. It can be seen from Figs. 8 and 15, the effect of rib height is monotonical while the effect of rib angle is non-monotonical. Therefore, it is essential to consider the combined effect of rib height and rib angle when optimizing the design of the V-shaped staggered rib cooling channel.

Taking the rib height of 2 mm and 1.5 mm as examples, the effect of rib angles on the flow field distribution in V-shaped staggered rib channels was studied. Fig. 16 shows the velocity distribution in the x-z plane for different rib angles. For rib height of 2 mm, the flow field distribution is most uniform at a 60° rib angle, with low velocity regions near the rib tips and sidewalls. At a 45° rib angle, the flow field shows significant high velocity regions and intense fluid mixing, especially near the upstream rib, where flow velocity peaks. According to Fig. 16, it is obvious that the V-shaped staggered rib can enhance cooling performance as a result of reduced low heat transfer region behind ribs and

Table 2
Structural parameters of channels with different rib angles.

Type	Number	Rib heights	Rid angles	Flow direction
V-shaped staggered ribs	1–9	0.5–4.5	60°	forward
	10–18	0.5–4.5	45°	forward
	19–27	0.5–4.5	37.5°	forward
	28–36	0.5–4.5	30°	forward

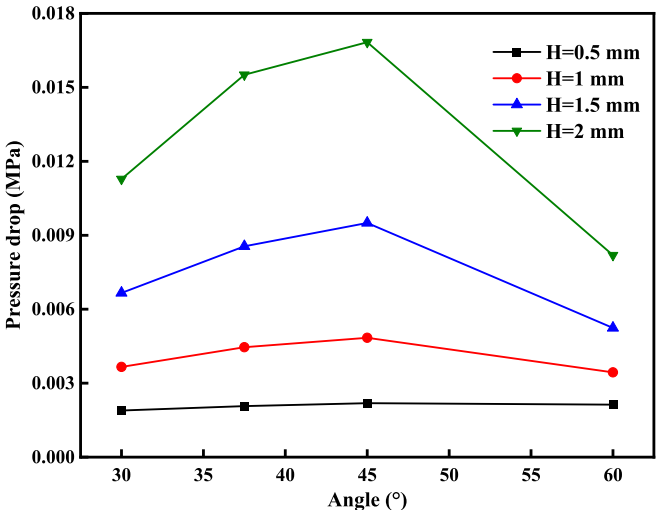

Fig. 15. The effect of rib angles on pressure drops.

enlarged high heat transfer region in front of ribs, which is also reported in Ref.[36,37]. When the fluid passes across the ribs, there will be low-pressure zones just downstream the ribs because of the flow separation, and the recirculation occurs in the low-pressure zones. As the rib angle changes, the area of recirculation zone changes [38]. The rib angle affects the vortex separation and mixing at the edge of the rib in the central area of channels, and also affects the size of the recirculation zone behind the rib. The flow field distribution and fluid mixing intensity at 37.5° and 30° rib angles between those at 60° and 45°. These variations in flow field structure and fluid mixing explain the differences in pressure drop, aligning with previous findings on the effect of rib angles on pressure drop. In addition, comparison of different rib heights shows that increasing rib height leads to more intense flow field mixing in the channel.

3.2.2. Heat transfer characteristic

The effect of rib angle on the maximum temperature of V-shaped staggered rib channels top wall is shown in Fig. 17. For rib heights of 0.5 mm and 1.0 mm, as the rib angle increases from 30° to 60°, the maximum surface temperature of V-shaped staggered rib channels decreases slowly and then increases rapidly. The lowest maximum surface temperature is observed at an angle of 45°, indicating the best heat transfer performance at this angle. However, for rib heights of 1.5 mm and 2.0 mm, the lowest maximum surface temperature occurs at an angle of 37.5°. Overall, the effect of rib angles on the maximum surface temperature of V-shaped staggered rib channels is non-monotonic, with a decreasing and then increasing trend from 30° to 60°. The rib height has a significant effect the lowest maximum surface temperature of V-shaped staggered rib channels. For rib height between 1.5 mm and 3.5 mm, the cooling effect is best at 37.5°, while for rib height between 0.5 mm and 1 mm, the cooling effect is optimal at 45°. Fig. 18 shows the effect of rib angles on the average Nu in a V-shaped staggered rib channels. It can be seen that with the increase in rib angle, the average Nu in V-shaped staggered rib channels initially increase and then decreases. When rib height is less than 1.5 mm, the average Nu reaches its maximum at a rib angle of 45°. However, when rib height exceeds 2 mm, the average Nu reaches its maximum at a rib angle of 37.5°.

As shown in Fig. 19, it can be seen that as rib angle increases the high temperature region gradually moves towards the outlet and becomes more uniform. When rib angle decreases from 60° to 45°, 37.5°, and 30°, the temperature changes on the top wall are significant. As the rib height increases, the high temperature region also gradually moves towards the outlet. The temperature distribution maps for 45°, 37.5°, and 30° show little difference, but the smaller the angle, the larger the high

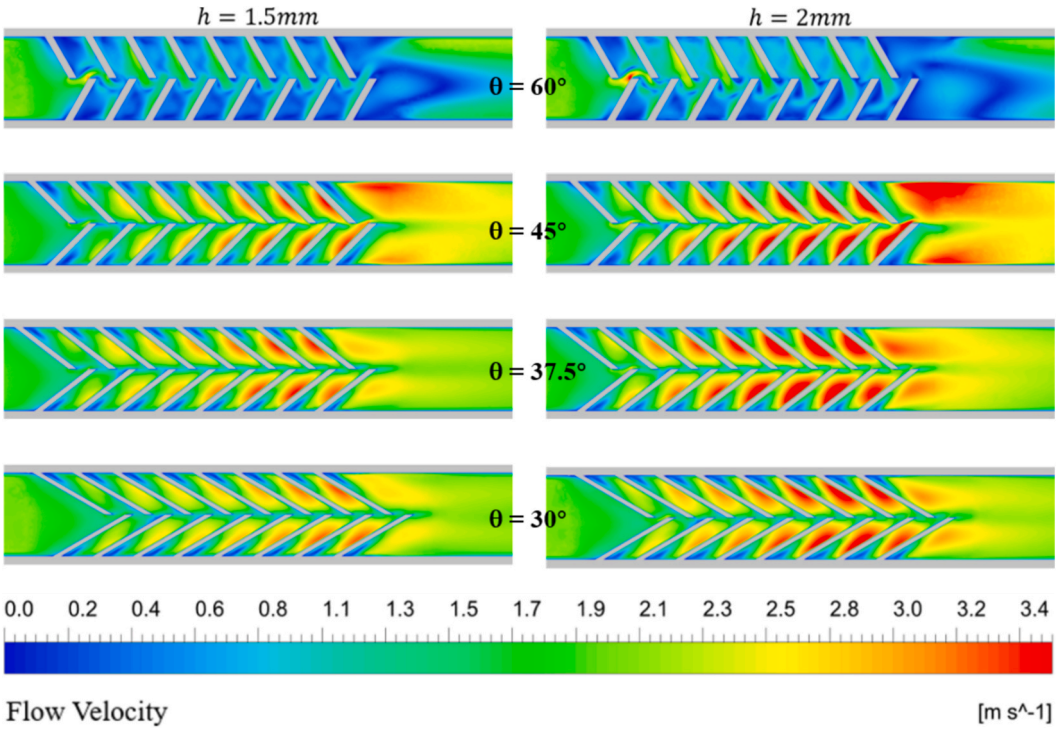

Fig. 16. The effect of rib angles on the velocity distribution (y = 6.5 mm).

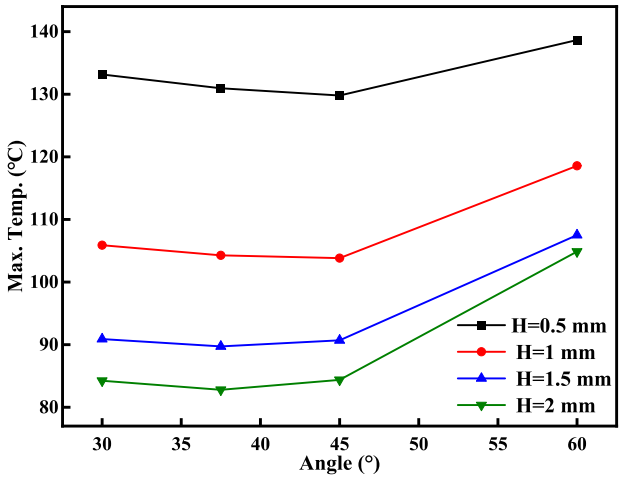

Fig. 17. The effect of rib angles on the maximum surface temperature.

temperature region. As analyzed in Fig. 16, on the back of the rib, the heat from the heating surfaces in recirculation zones cannot be transferred to the mainstream quickly, these zones correspond to the low heat transfer regions and high temperature regions, similar phenomenon are also reported in Ref [36–38].

3.2.3. *Thermal-hydraulic performance factor*

Fig. 20 shows the effect of the angle of V-shaped staggered ribs on the thermal–hydraulic performance factor. It can be seen that when rib height is greater than 1.5 mm, the thermal–hydraulic performance factor decreases with an increase in rib angle. However, for rib heights of 0.5 mm and 1.0 mm, the effect of rib angles is more complex. Specifically, for a rib height of 1.0 mm, the thermal–hydraulic performance factor reaches its maximum at a rib angle of 45°, while for a rib height of 0.5 mm, it peaks at a rib angle of 60°. Considering the effects of rib heights and angles on the convection heat transfer performance and pressure drop of the V-shaped staggered rib channels, smaller rib height and angle generally result in a higher thermal–hydraulic performance factor. However, when rib height exceeds 3.0 mm, the significant increase in pressure drop causes the comprehensive thermal–hydraulic performance factor to fall below 1. Overall, the effect of rib heights on the thermal–hydraulic performance factor is more significant than that of rib angle.

To sum up, the effect of rib angle on pressure drops, average Nu number, surface temperature, flow field distribution and heat transfer process of the V-shaped staggered rib channels is complicated and non-monotonic. The effect mechanism of the rib angle is inferred that the rib angle affects the vortex separation and mixing at the edge of the rib, and also affects the size of the recirculation zone area behind the rib, which affects the mass and heat transfer process in the central area and the recirculation area in the channel, and then affects the flow and heat transfer performance. In general, as the rib angle increases, the pressure

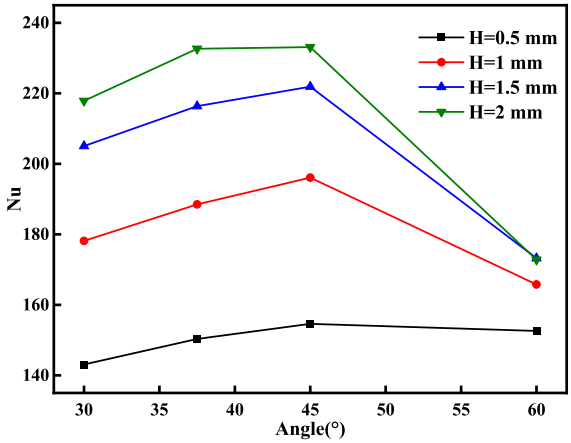

Fig. 18. The effect of rib angles on the average Nu.

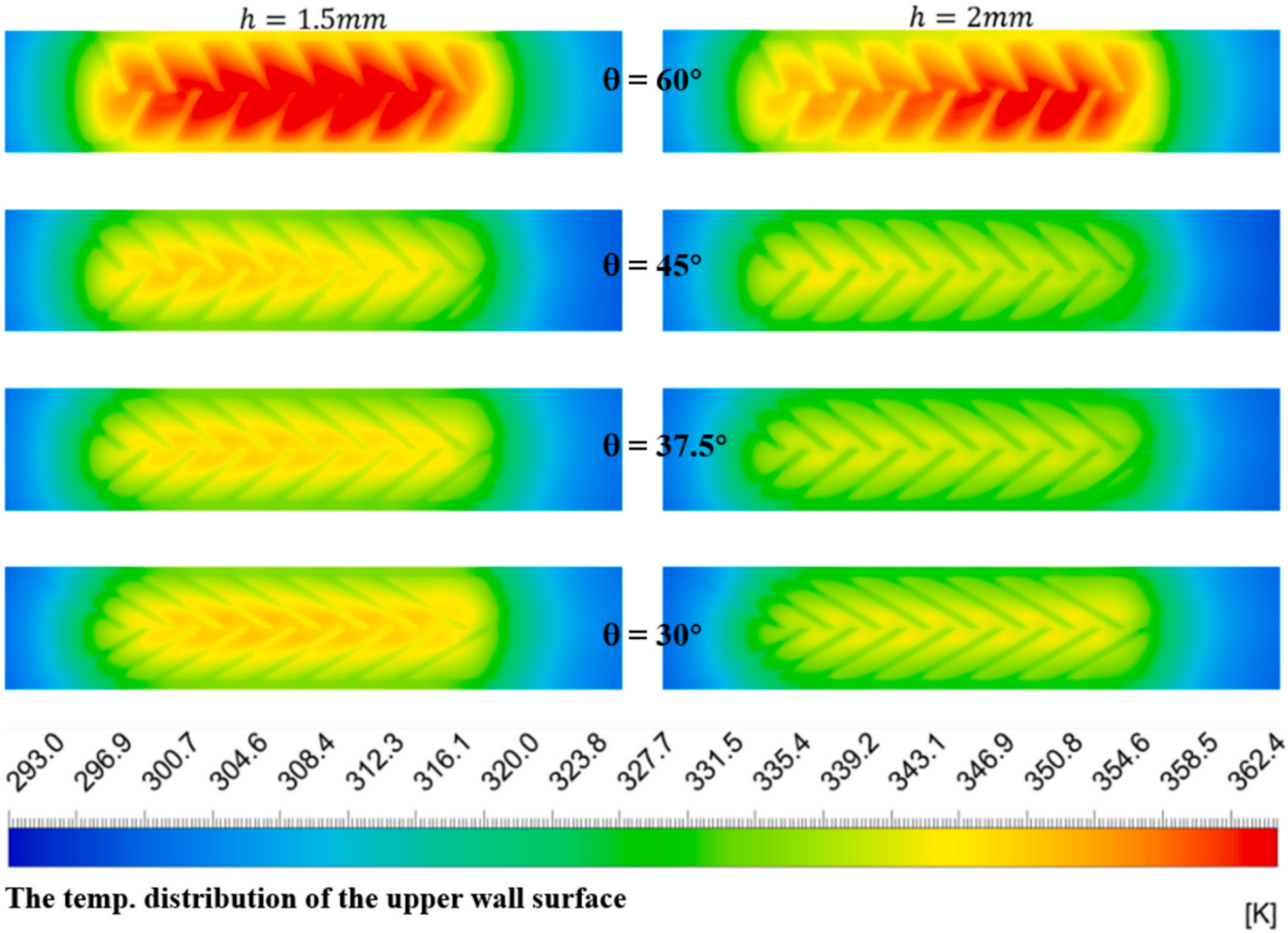

Fig. 19. The effect of rib angles on the temperature distribution of wall surface.

drops increase, the heat transfer capacity increases, and the wall temperature decreases. The optimum rib angle is about 45° (just in the ranges of this study). When the rib angle continues increasing (above 45°), the heat transfer efficiency decreases, the wall temperature increases, and the pressure drop decreases. However, from the view of the effect of rib height, the optimum rib angle is different. For example, in the condition of 2 mm rib height, the optimum rib angle is 40°, while in the conditions of rib height lower than 2 mm, the optimum rib angle is 45°. From the perspective of mechanism research and practical application, it is very valuable to carry out structural optimization research under the effects of the superposition of rib angle and rib height.

3.3. *Effect of flow direction*

On the basis of the above discussion, the effect of forward and backward flow directions on the flow and heat transfer characteristics in

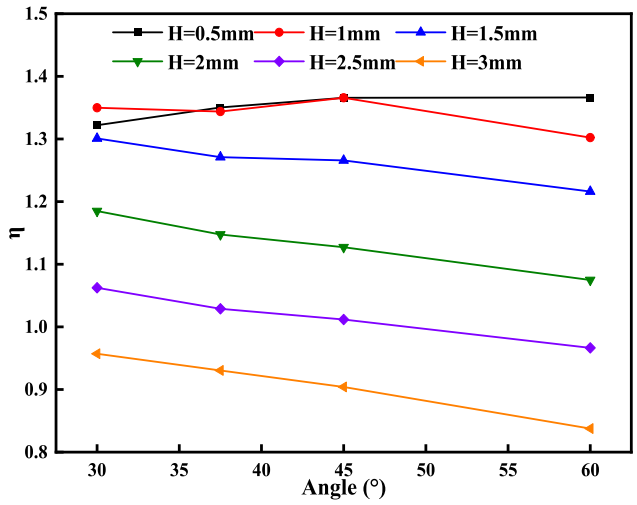

Fig. 20. The effect of rib angles on the thermal–hydraulic performance factor.

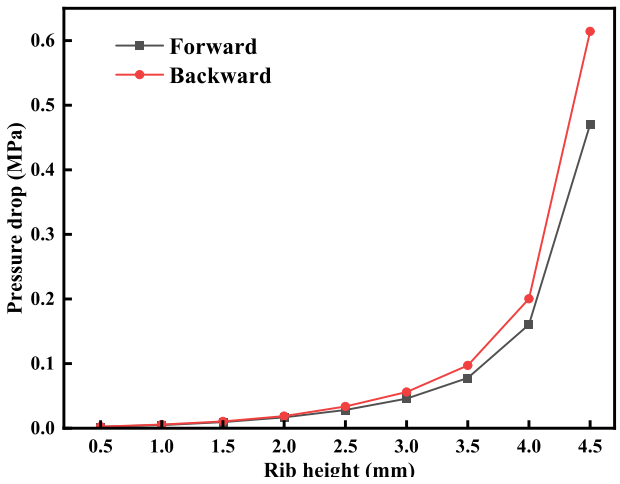

Fig. 21. The effect of flow direction on pressure drops.

V-shaped staggered rib channels with rib angles of 45° was analyzed in this section. A total of 18 working conditions were simulated with specific parameter settings as shown in Table 3.

3.3.1. *Flow field characteristic*

The effect of different flow directions on the pressure drop is illustrated in Fig. 21, with rib heights ranging from 0.5 mm to 4.5 mm. It is evident that as rib height increases, the pressure drop for both forward and backward flows show an increasing trend. In addition, the pressure drop for backward flow consistently exceeds that of forward flow. Moreover, as rib height increases, the disparity between forward and backward flow also grows. For example, when rib height is 1.5 mm, the pressure drop between the inlet and outlet for backward flow is 10 % higher than that for forward flow. Similarly, when rib height is 2 mm, the pressure drop between the inlet and outlet for backward flow increases by 12 % compared to forward flow.

Taking rib heights of 1.5 mm and 2 mm as examples, the effect of flow directions on the flow field distribution in V-shaped staggered rib channels is analyzed. The velocity distribution in the x-z plane for different flow directions is shown in Fig. 22. Both forward and backward flows create high-velocity regions at the outlet of V-shaped staggered rib channels. Backward flow results in a distinct low-velocity region at the inlet of the V-shaped staggered rib channels. For backward flow, the low-velocity region near the sidewalls is smaller, and the high-velocity region between the ribs is larger. Unlike forward flow, backward flow generates a wave-like high-velocity region near the rib tips in the central area. The wave-like high-velocity region from backward flow effectively disrupts the velocity boundary layer along the channel sidewalls.

3.3.2. *Heat transfer characteristic*

Fig. 23 illustrates the maximum surface temperature in V-shaped staggered rib channels under various flow directions. It is evident that for rib heights less than 3 mm, backward flow is more effective in reducing the maximum surface temperature. As rib height increases, this difference diminishes significantly. At a rib height of 3 mm, the difference in maximum surface temperature between forward and backward flow is approximately 0.1 °C. Specifically, at rib heights of 1.5 mm and 2 mm, the maximum surface temperatures in backward flow are 4 % and 2 % lower, respectively, compared to forward flow.

Fig. 24 shows the variation of the average Nusselt number of V-shaped staggered rib channels under different flow directions. It can be observed that the average Nu is higher for backward flow compared to forward flow when rib heights are 0.5 mm and 1 mm. However, for rib heights exceeding 1.5 mm, the average Nu is higher for forward flow. The average Nu for backward flow peaks at 2.5 mm for rib heights ranging from 0.5 mm to 4.5 mm, while the rate of increase in the average Nu for forward flow gradually decreases with increasing rib height.

Taking rib heights of 1.5 mm and 2 mm as examples, the temperature distribution on the top wall of V-shaped staggered rib channels under different flow directions is illustrated in Fig. 25. The results indicate that the average top wall temperature is lower in backward flow compared to forward flow. Both forward and backward flow directions generate high-temperature regions at the inlet, which correspond to the velocity distribution. Moreover, the temperature distribution between ribs is more uniform in backward flow, whereas forward flow shows a significant temperature gradient. As rib height increase, the high-temperature regions in backward flow are smaller compared to those in forward flow.

3.3.3. *Thermal-hydraulic performance factor*

Fig. 26 shows the effect of different flow directions on the thermal–hydraulic performance factor in a V-shaped staggered rib channel. It is evident that as rib height increases, the thermal–hydraulic performance factor decreases for both flow directions, with a more significant reduction in the backward flow direction compared to the forward flow direction. In the range of 0.5 mm to 2.5 mm, the thermal–hydraulic performance factor (η) for forward flow is consistently above 1, reaching a maximum value of 1.366 at 0.5 mm. For backward flow, the thermal–hydraulic performance factor is above 1 in the range of 0.5 mm to 2 mm, with a maximum value of 1.358 at 0.5 mm. From the perspective of the thermal–hydraulic performance factor, forward flow outperforms backward flow. As the maximum temperature, backward flow enhances the cooling of V-shaped staggered rib channels, resulting in a further decrease in the maximum surface temperature. However, in terms of thermal–hydraulic performance factors, the cooling effectiveness of backward flow is not as high as that of forward flow. Nevertheless, the disparity between the two is not substantial. Hence, it is worth contemplating sacrificing some cooling efficiency to attain a lower maximum temperature.

Based on the comparative analysis of the rib height, rib angle and flow direction of the V-shaped staggered rib, as well as the comparison with the straight rib and smooth channel, some conclusions and mechanism can be summarized as follows. Compared to traditional straight ribs and continuous wavy structures, the V-shaped staggered rib structure guides vortex formation in local flow fields, promotes lateral

Table 3
Structural parameters of channels with different flow directions.

Type	Number	Rib height	Rib angle	Flow direction
V-shaped staggered ribs	1–9	0.5–4.5	45°	Forward
	10–18	0.5–4.5	45°	Backward

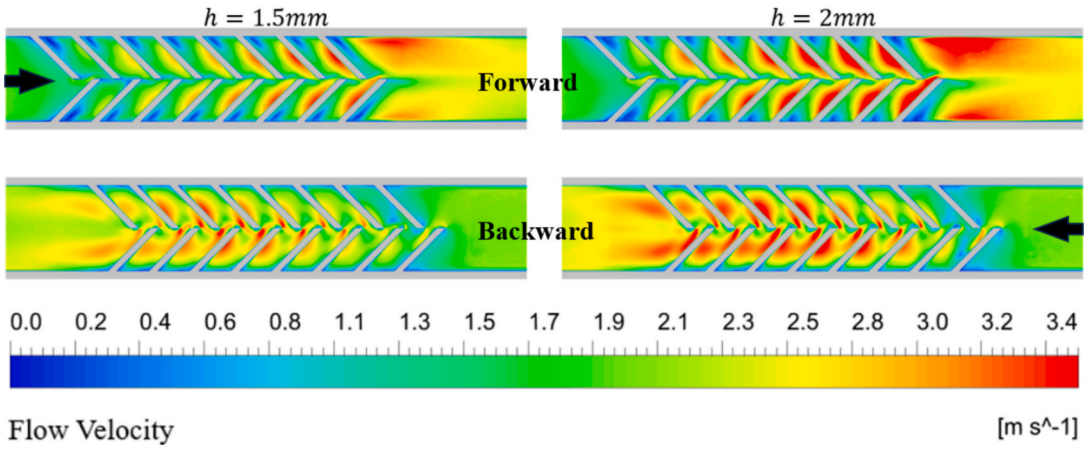

Fig. 22. The effect of flow directions on the velocity distribution.

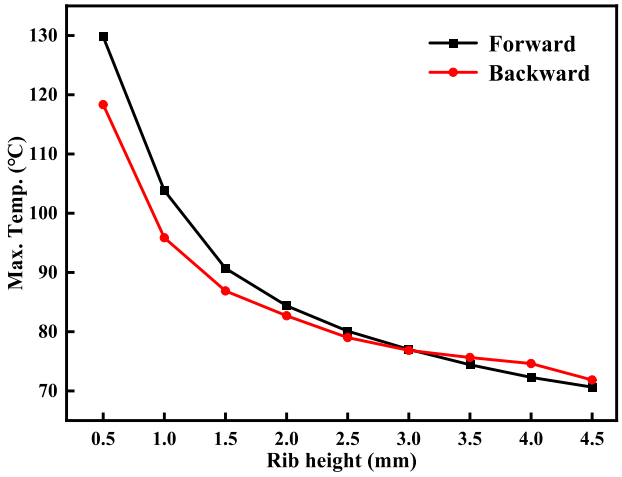

Fig. 23. The effect of flow direction on the maximum surface temperature.

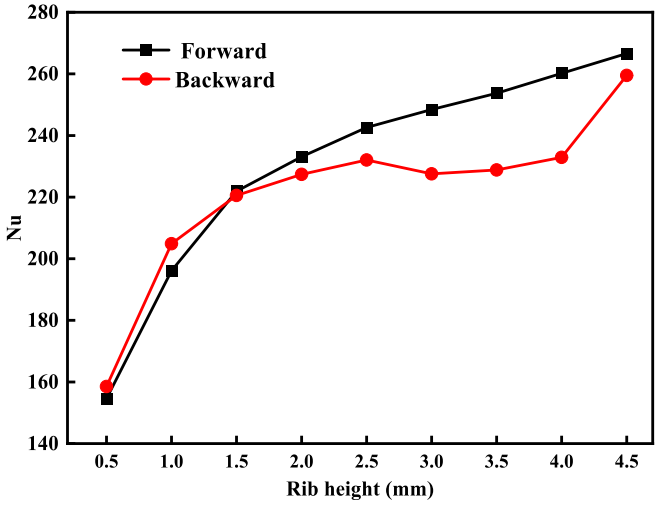

Fig. 24. The effect of flow direction on the average Nu.

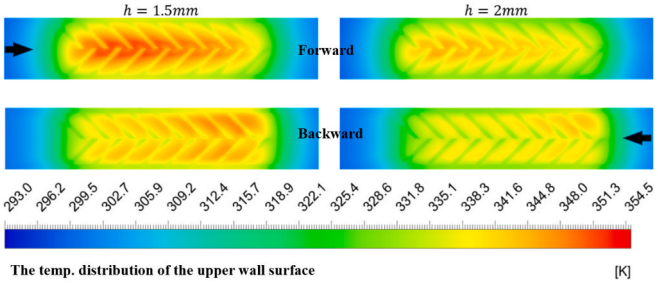

Fig. 25. The temperature distribution with different flow directions.

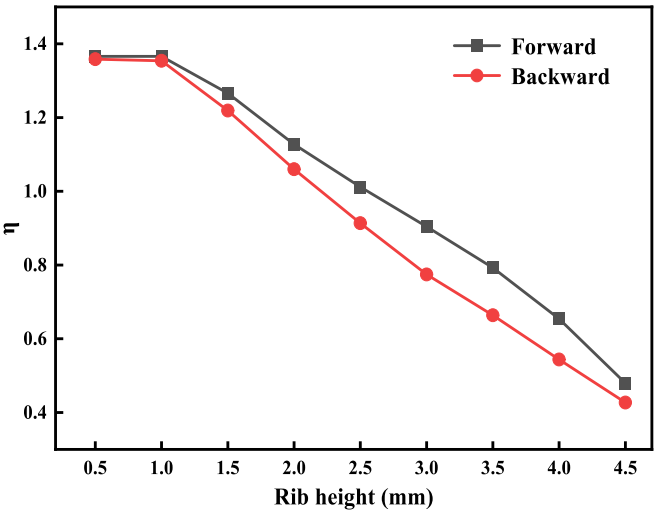

Fig. 26. The effect of flow direction on the thermal–hydraulic performance factor.

mixing, and significantly reduces pressure drop penalties, thereby achieving a superior balance between heat transfer enhancement and pressure drop control. Furthermore, the advantages of the V-shaped staggered rib structure are not limited to its ability to enhance heat transfer and control pressure drop but also include its high engineering feasibility and adaptability. First, the geometry of this structure is relatively simple, making it easy to manufacture using conventional fabrication techniques and reducing implementation costs. Second, the V-shaped staggered ribs demonstrate excellent turbulence enhancement under various flow conditions, enabling them to adapt to complex working environments and meet diverse application needs. Additionally, this structure effectively regulates the flow field by optimizing the rib arrangement, improving heat transfer efficiency, reducing the formation of localized hot spots, and enhancing the overall operational reliability of the system. Therefore, the V-shaped staggered rib structure

not only provides new insights into heat transfer enhancement research but also offers significant theoretical support and practical solutions for the design of efficient and economical heat exchange structures in real-world engineering applications.

4. Conclusions

To address the heat dissipation challenges of the BNCT solid-state Li target, this study designed a V-shaped staggered rib channel structure and conducted numerical simulations to evaluate its flow and heat transfer performance under different rib heights, rib angles, and flow directions. Some conclusions are as follows:

(1) The effect of rib height on the heat transfer capability and pressure drop is monotonous. As the rib height increases, the pressure drops increases and the heat transfer coefficient increases. The mechanism is that on the one hand the flow cross-sectional area decreases and the flow rate increases with the rib height increasing; on the other hand, the flow shear, flow separation and vortex separation of the flow layer in the central of the channel lead to more intense fluid mixing, thus strengthening the mass and heat transfer performance.
(2) The effect of rib angle on the heat transfer process and pressure drop of is non-monotonic and reaches the optimal value at about 45°. The mechanism is inferred to be that the rib angle affects the fluid shear and flow separation at the rib edge, and the downstream vortex separation and mixing, etc. Besides, the rib angle also affects the size and area of the recirculation zone behind the rib, and thus affects the fluid mixing and heat transfer process in the channel.
(3) The V-shaped staggered rib channel significantly improved heat dissipation. At a rib angle of 60° and rib height of 2 mm, the maximum surface temperature of the Cu substrate was reduced to 104 °C, representing a 48 % reduction compared to the smooth channel and a 26 % reduction compared to the straight ribbed channel. At a 37.5° angle at a rib height of 2 mm achieved the lowest surface temperature of 82.8 °C, a 70 % reduction compared to the straight ribbed channel. However, the reduction in the thermal–hydraulic performance factor, indicates a design trade-off that must be managed to maintain system efficiency and operational reliability.

In the present study, the V-shaped staggered rib structure was selected to balance engineering feasibility and heat transfer performance. By effectively reducing surface temperatures and improving thermal management, the V-shaped staggered rib design directly addresses the heat dissipation challenges of BNCT solid-state Li targets. With the advancement of additive manufacturing technology, future research could exploit its capabilities to create more complex geometries (for example TPMS structure), overcoming the limitations of traditional manufacturing and developing structures with improved heat transfer performance, thereby further improving thermal management.

Declaration of competing interest

The authors declare that they have no known competing financial interests or personal relationships that could have appeared to influence the work reported in this paper.

Acknowledgments

This work was supported by the National Natural Science Foundation of China (Grant No. 12105142), the Aeronautical Science Fund (Grant No. 20240058052004), the Fundamental Research Funds for the Central University (Grant No. 56XCA2402601), the Graduate Research Innovation Program Project of Jiangsu Province (Grant No. KYCX24_0617).

Data availability

Data will be made available on request.

References

[1] S. Nakamura, M. Takemori, T. Nakaichi, et al., A method for delivering the required neutron fluence in an accelerator-based boron neutron capture therapy system employing a lithium target[J], Sci. Rep. 14 (1) (2024) 11253.
[2] S. Nakamura, H. Igaki, H. Okamoto, et al., Dependence of neutrons generated by 7Li (p, n) reaction on Li thickness under free-air condition in accelerator-based boron neutron capture therapy system employing solid-state Li target[J], Phys. Med. 58 (2019) 121–130.
[3] A.J. Kreiner, J. Bergueiro, D. Cartelli, et al., Present status of accelerator-based BNCT[J], Reports of Practical Oncology & Radiotherapy 21 (2) (2016) 95–101.
[4] C. Willis, J. Lenz, D. Swenson, High-power lithium target for accelerator-based BNCT[J], Proceedings of LINAC08 (2008) 223–225.
[5] S. Nakamura, H. Igaki, M. Ito, et al., Characterization of the relationship between neutron production and thermal load on a target material in an accelerator-based boron neutron capture therapy system employing a solid-state Li target[J], PLoS One 14 (11) (2019) e0225587.
[6] X. Li, Y. Ikeda, T. Kobayashi, et al., Study on the edge-cooling target structure for transportable accelerator-driven neutron source[J], Nucl. Instrum. Methods Phys. Res., Sect. A 1017 (2021) 165793.
[7] W. Junyan, K. Haiyun, L. Deming, Design of a neutron target for boron neutron capture therapy (in Chinese), Nucl. Tech. 47 (04) (2024) 34–40.
[8] Y. Hu, X. Li, Y. Lv, et al., Simulations on the thermal and mechanical performance of the rotating target system of accelerator-driven neutron source for Boron Neutron Capture Therapy (BNCT)[J], Nucl. Instrum. Methods Phys. Res., Sect. A 1053 (2023) 168340.
[9] H. Yu, T. Li, X. Zeng, et al., A critical review on geometric improvements for heat transfer augmentation of microchannels[J], Energies 15 (24) (2022) 9474.
[10] Y. Lin, Y. Luo, W. Li, et al., Enhancement of flow boiling heat transfer in microchannel using micro-fin and micro-cavity surfaces[J], Int. J. Heat Mass Transf. 179 (2021) 121739.
[11] A.J. Chamkha, M. Molana, A. Rahnama, et al., On the nanofluids applications in microchannels: a comprehensive review[J], Powder Technol. 332 (2018) 287–322.
[12] L. Chai, R. Shaukat, L. Wang, et al., A review on heat transfer and hydrodynamic characteristics of nano/microencapsulated phase change slurry (N/MPCS) in mini/microchannel heat sinks[J], Appl. Therm. Eng. 135 (2018) 334–349.
[13] L. Huang, J. Zou, B. Liu, et al., Machine learning assisted microchannel geometric optimization—a case study of channel designs[J], Energies 17 (1) (2023) 44.
[14] I.A. Ghani, N. Kamaruzaman, N.A.C. Sidik, Heat transfer augmentation in a microchannel heat sink with sinusoidal cavities and rectangular ribs[J], Int. J. Heat Mass Transf. 108 (2017) 1969–1981.
[15] S. Pourhammati, S. Hossainpour, Improving the hydrothermal characteristics of wavy microchannel heat sink by modification of wavelength and wave amplitude [J], Int. Commun. Heat Mass Transfer 130 (2022) 105805.
[16] M. Ghorbani, M.R. Salimpour, K. Vafai, Microchannel thermal performance optimization utilizing porous layer configurations[J], Int. J. Heat Mass Transf. 133 (2019) 62–72.
[17] D. Deng, L. Zeng, W. Sun, A review on flow boiling enhancement and fabrication of enhanced microchannels of microchannel heat sinks[J], Int. J. Heat Mass Transf. 175 (2021) 121332.
[18] C.G.J. Prakash, R. Prasanth, Enhanced boiling heat transfer by nano structured surfaces and nanofluids[J], Renew. Sustain. Energy Rev. 82 (2018) 4028–4043.
[19] S. Rashidi, F. Hormozi, B. Sundén, et al., Energy saving in thermal energy systems using dimpled surface technology–a review on mechanisms and applications[J], Appl. Energy 250 (2019) 1491–1547.
[20] S.L. Wang, D. An, Y.R. Yang, et al., Heat transfer and flow characteristics in symmetric and parallel wavy microchannel heat sinks with porous ribs[J], Int. J. Therm. Sci. 185 (2023) 108080.
[21] J. Wang, X. Yang, J.J. Klemeš, et al., A review on nanofluid stability: preparation and application[J], Renew. Sustain. Energy Rev. 188 (2023) 113854.
[22] N.I. Ibrahim, F.A. Al-Sulaiman, S. Rahman, et al., Heat transfer enhancement of phase change materials for thermal energy storage applications: a critical review [J], Renew. Sustain. Energy Rev. 74 (2017) 26–50.
[23] L. Guoqing, Z. Shaofei, Y. Yanru, et al., Fluid flow and heat transfer of ribbed channel based on the hierarchical design concept[J], J. Aerospace Power 39 (10) (2024) 20220861.
[24] M. Otto, J. Kapat, M. Ricklick, et al., Heat transfer in a rib turbulated pin fin array for trailing edge cooling[J], J. Therm. Sci. Eng. Appl. 14 (4) (2022) 041012.
[25] K.A.A. Ramadan, K.V. Slyusarskiy, Effect of fin type and geometry on thermal and hydraulic performance in conditions of combined-cycle nuclear power plant with high-temperature gas-cooled reactors[J], Thermo 4 (3) (2024) 382–393.
[26] P. Promvonge, W. Changcharoen, S. Kwankaomeng, et al., Numerical heat transfer study of turbulent square-duct flow through inline V-shaped discrete ribs[J], Int. Commun. Heat Mass Transfer 38 (10) (2011) 1392–1399.
[27] V. SriHarsha, S.V. Prabhu, R.P. Vedula, Influence of rib height on the local heat transfer distribution and pressure drop in a square channel with 90 continuous and 60 V-broken ribs[J], Appl. Therm. Eng. 29 (11–12) (2009) 2444–2459.
[28] L. Zhaoxuan, Z. Chengbin, H. Qun, et al., Numerical simulation of fluid flow and heat transfer characteristics in a saw-like microchannel (in Chinese), Chemical Industry and Engineering Progress 42 (11) (2023) 5622–5636.

[29] Z. Aiping, B. Shuai, F. Lei, Numerical simulation of the flow and heat transfer in a straight channel installed inside with V-shaped Ribs (in Chinese), J. Eng. Thermal Energy and Power 30 (02) (2015) 205–211.
[30] W. Rong, M. Keke, H. Chang, Study on heat transfer characteristics of V-shaped discrete ribs in turbine blade passage (in Chinese), J. Aerospace Power 38 (12) (2023) 2817–2828.
[31] S. Yoshihashi, T. Tsuneyoshi, K. Tsuchida, et al., High heat removal technique for a lithium neutron generation target used for an accelerator-driven BNCT system[J], J. Instrum. 16 (04) (2021) P04016.
[32] L. Peiyi, T. Xiaobin, G. Changran, et al., A bi-tapered and air-gapped beam shaping assembly used for AB-BNCT[J], Appl. Radiat. Isot. 167 (2021) 109392.
[33] Y. Fang, H. Qin, C. Wang, et al., Numerical investigation on thermohydraulic performance of high temperature hydrogen in twisted rod channels[J], Ann. Nucl. Energy 161 (2021) 108434.
[34] D.H. Kong, W.B. Chen, X.Y. Niu, et al., A comparative study of internal heat transfer enhancement of impingement/effusion cooling roughened by solid rib and slit rib[J], Phys. Fluids 36 (1) (2024) 015106.
[35] Q. Zhu, Y. Jin, J. Chen, et al., Computational study of rib shape and configuration for heat transfer and fluid flow characteristics of microchannel heat sinks with fan-shaped cavities[J], Appl. Therm. Eng. 195 (2021) 117171.
[36] N. Zheng, W. Liu, Z. Liu, et al., A numerical study on heat transfer enhancement and the flow structure in a heat exchanger tube with discrete double inclined ribs [J], Appl. Therm. Eng. 90 (2015) 232–241.
[37] S.Y. Ran, P. Zhang, Y. Rao, Numerical study of heat transfer and flow structure over channel surfaces featuring miniature V rib-dimples with various configurations[J], Int. J. Therm. Sci. 172 (2022) 107342.
[38] H. Li, T. Yu, D. Wang, et al., Heat-transfer enhancing mechanisms induced by the coherent structures of wall-bounded turbulence in channel with rib[J], Int. J. Heat Mass Transf. 137 (2019) 446–460.